Ordered organic-organic multilayer growth

Richard R. Lunt, Kai Sun, Michael Kröger, J. B. Benziger, and Stephen R. Forrest

Phys. Rev. B **83**, 064114 — Published 28 February 2011

DOI: 10.1103/PhysRevB.83.064114

Ordered Organic-Organic Multilayer Growth

Richard R. Lunt[a,b], Kai Sun [c], Michael Kröger[d], Jay B. Benziger[a], and Stephen R. Forrest[b), c)]

[a)]Department of Chemical Engineering, Princeton Institute for the Science and Technology of Materials (PRISM), Princeton University, Princeton, NJ 08544 USA

[b)]Departments of Electrical Engineering & Computer Science, Physics, and Materials Science & Engineering, University of Michigan, Ann Arbor, Michigan 48109 USA

[c)]Department of Material Science and Engineering,
University of Michigan, Ann Arbor, MI 48109 USA

[d)] InnovationLab GmbH, Speyerer Straße 4, 69115 Heidelberg, Germany

stevefor@umich.edu

Abstract

Crystalline order and orientation influence both the electronic and optical properties of thin organic crystalline films. Here, we demonstrate the quasi-epitaxially ordered growth via organic vapor phase deposition of two organic materials, 1,4,5,8-naphthalene-tetracarboxylic-dianhydride (NTCDA), and dibenzotetrathiafulvalene-tetracyanoquinodimethane (DB-TCNQ) on single crystal substrates. To understand the quasi-epitaxial orientations between the organic-inorganic and organic-organic lattices we compare geometrical lattice registry to full-structure van der Waals potential calculations, and find that only the complete description of the atomistic potential correctly matches experimentally observed orientations. We also demonstrate single crystalline film growth of alternating multiple quasi-epitaxial layers of these two organic

semiconductors, and discuss this phenomenon in the context of incommensurate quasiepitaxy and surface energy matching, which is distinct from the lattice-matching criterion for inorganic heteroepitaxy.

I. INTRODUCTION

The growth of ordered crystalline organic layers has been of long standing interest for the improvement of organic optoelectronic device performance. By analogy, crystalline inorganic epitaxial heterostructures and quantum wells are ubiquitous features of state-of-the art optoelectronic devices. While there are number of examples of organic epitaxy on inorganic substrates, much less is known about crystalline ordering of organic-organic epitaxy. In part, this is due to difficulties associated with growing highly ordered organic-organic heterojunctions. Nonetheless, recent studies have explored these relationships in several small molecule materials combinations[1-6]. In many cases, no clear commensurability was found, although so-called coincident epitaxy was reported.[4] Observations of sustained ordered multilayer heteroepitaxial growth have been infrequent, possibly due to deposition-order anisotropies[7]. For example, a recent study showed that a highly ordered quasi-epitaxial[8] copper phthalocyanine (CuPc) layer could be grown on crystalline layers of 3,4,9,10 perylenetetracarboxylic dianhydride (PTCDA), while the reverse growth order (PTCDA on CuPc) leads to small grain powder formation[7]. One of the few examples of successful multilayer heteroepitaxial growth was studied by Forrest, et al. using multilayers of 1,4,5,8-naphthalene-tetracarboxylic-dianhydride (NTCDA)(2nm)/PTCDA(2nm) grown with up to two polycrystalline pairs by organic molecular beam deposition (OMBD).[9-11] Here, we demonstrate the quasiepitaxial ordering of NTCDA and the neutral charge transfer complex[12], dibenzotetrathiafulvalene (DB)-tetracyanoquinodimethane (TCNQ), multilayers grown on crystalline substrates via organic vapor-phase deposition (OVPD)[13]. Sustained ordering of NTCDA/DB-TCNQ pairs was maintained for > 5 periods, with a clear quasi-epitaxial relationship between

adjacent layers in the stacks. We discuss both the potential energy minimization that leads to quasiepitaxial alignment, and the symmetric growth-order phenomenon in terms of crystal-surface energy matching.

II. THEORY

Atomistic van der Waals potential energies were calculated and summed between adlayer and substrate with a custom Matlab code without simplification of the molecular potential.[14] The full atom-atom potentials were calculated using a 6-12 Lennard-Jones (LJ) potential, where pure component LJ constants in Table I were obtained from Material Studio *v*4.1 for hybridized carbon, oxygen, sulfur, nitrogen, bromine, and potassium ion. The atomic LJ potential is:

$$\phi_{ij} = A_{ij}\left(\left(\frac{B_{ij}}{r}\right)^{12} - \left(\frac{B_{ij}}{r}\right)^{6}\right), \qquad (1)$$

where r is the separation distance between atom i and j, A_{ij} is the potential depth, and B_{ij} is the atomic interaction distance. For unlike atomic interactions, geometric and arithmetic mixing rules were used to calculate A and B, respectively. The potential was summed over all adlayer-substrate atom combinations up to a distance of 1nm for a single monolayer (ML) of adlayer with one ML of substrate as:

$$\Theta = \sum_{i}^{n_a}\sum_{j}^{n_s}\phi_{ij}, \qquad (2)$$

where n_s is the number of atoms in the substrate and n_a is the number of atoms in the adlayer. The rotation angle (θ) was defined as the angle between b_1 of the adlayer and substrate (i.e. short axes of the NTCDA and DB-TCNQ unit cells). The potential energy (PE) was calculated as a function of substrate-adlayer distance to find the equilibrium

separation, and was then calculated as the adlayer was translated across two full unit cells of the substrate to find the PE minimum at each rotation angle, θ. Calculations were repeated for surface mesh sizes of 3*x*3 and 15*x*15 adlayer unit meshes over 15*x*15 and 51*x*51 substrate unit meshes, respectively, to avoid edge effects.

To test the validity of the van der Waals description of the molecular bonding (particularly for DB-TCNQ, where electrostatic forces may make a contribution to the total energy) the equilibrium van der Waals separation distance between individual molecules of DB and TCNQ, and between DB-TCNQ pairs were calculated and compared to the values determined from the experimental crystal structure. In both cases, these separation distances, 0.329nm and 0.327nm respectively, are in good agreement and indicate that other (non-van der Waa;s) contributions to the potential are negligible. In addition, a similar calculation was made for PTCDA, where the calculated and experimental equilibrium separation distances are found to be 0.320 nm and 0l.321 nm, respectively, also well within experimental error.

Surface energy calculations incorporating summation of intralayer interactions, were calculated separately with periodic boundary conditions for a range of organic crystals and crystal planes.[15] For comparison, geometric lattice potential (i.e. lattice registry) was evaluated as a function of θ according to the method of Hillier and Ward[16], where each lattice is assigned a sinusoidal potential so that the dimensionless potential (V/V_0) describes the degree of lattice commensurism; V/V_0 of 1.0, 0.5, and 0.0 indicate incommensurate, concident, and commensurate lattices, respectively. For this simplified model, the lattice is rotated around a fixed point on the unit cell (i.e. without translation),

since the calculation only explores lattice commensurism and requires more than one overlapping lattice points for $V/V_0 < 1$.

III. EXPERIMENTAL

NTCDA is a wide-optical bandgap (3.1eV) small molecular weight semiconductor[17], and DB-TCNQ is a neutral semiconducting charge transfer complex[18-20] with a comparatively small optical bandgap (~0.6eV measured by optical spectroscopy). DB-TCNQ was prepared by mixing hot solutions of tetrahydrofuran with dissolved DB and TCNQ (with molar ratio DB to TCNQ of 1:1), upon which shiny black crystals precipitated. DB-TCNQ was used without further purification, while commercially obtained NTCDA[21] was purified twice by gradient sublimation[22]. Each material was loaded into separate boats in a multi-barrel OVPD system equipped with *in-situ* high pressure reflection high energy electron diffraction (HP-RHEED)[13, 23]. For these studies, HP-RHEED is useful for monitoring both the crystal structure and quality of each layer before it is buried under the next. All layers were grown with a nitrogen background pressure of 10 mTorr and source flow rate of 25sccm (standard cubic centimeters per minute) on single crystal KBr substrates cleaved prior to growth. Thicknesses and deposition rates were measured *in-situ* with a quartz crystal microbalance calibrated with an *ex-situ* variable-angle spectroscopic ellipsometer. The substrate temperature was varied between -40ºC and 90ºC, and deposition rates were between 0.05 and 0.4nm/s. Crystalline growth was monitored in real-time via in-situ HP-RHEED at a beam energy and current of 20keV and <0.1 μA to avoid beam damage. In-plane lattice constants were measured from HP-RHEED patterns using the initial KBr diffraction pattern as a

reference. Uncertainties for orientation matrices were propagated from the uncertainty of the measured lattice spacings and rotation angles. Ex-situ Bragg-Brentano x-ray diffraction measurements were preformed in a rotating anode diffractometer with a CuK_α source to determine the out-of-plane molecular crystal spacing and orientation. Selected area electron diffraction (SAED) patterns were taken using a JEOL 3011 transmission electron microscope (TEM) operated at 300 keV with the organic layers mounted on a Cu grid after aqueous dissolution of the underlying KBr substrate. The growth of each layer was optimized around growth conditions leading the most well-defined and longest RHEED streak patterns. Optimum growth conditions for NTCDA were substrate temperatures between 10ºC and 35ºC, and growth rates between 0.05 nm/s and 0.15 nm/s, while for DB-TCNQ these conditions were between -10ºC and 10ºC, and 0.15 nm/s and 0.4 nm/s; several minutes between each growth was required to change the substrate temperature.

IV. RESULTS

Figure 1 shows the HP-RHEED patterns for the multilayer growth of NTCDA/DB-TCNQ. Similar to growth on PTCDA[9], NTCDA grows on KBr with its (100) plane perpendicular to the substrate. For (100) NTCDA, the molecules are positioned in lengthwise contact with the substrate, in an in-plane herringbone structure (see Fig. 1 right). The HP-RHEED patterns of the first layer of NTCDA and the second layer (fourth layer overall) of DB-TCNQ are shown in Fig. 2 for various rotations. The diffraction patterns vary along different azimuthal angles corresponding to different crystal directions in the NTCDA lattice, indicating single-crystalline ordered growth

across the substrate (~ 2 *x* 2cm^2). Additionally, the diffraction patterns exhibit long unbroken streaks indicative of a flat surface, from which we infer a layer-by-layer growth mode. The bulk lattice of NTCDA(100) has unit mesh dimensions of b_1 = 0.531nm, b_2 = 1.257nm, and β = 90º. From the RHEED data, we measure b_1 = 0.497(±0.005)nm, and b_2 = 1.31(±0.01)nm for the first layer, which is slightly reconstructed from the bulk phase, but nearly identical to the observations made for (100) NTCDA grown on crystalline PTCDA on HOPG.[9]

From the x-ray diffraction (XRD) data in Fig. 3, we measure an out-of-plane *d*-spacing of $d_{(100)}$ = 0.745(±0.003)nm, which is slightly compressed compared to the bulk spacing of $d_{(100)}$ = 0.751(±0.001)nm, indicating tetragonal distortion. The in-plane NTCDA lattice constants were not found to vary for neat-film growth of thicknesses up to 100 nm, suggesting that although the lattice is reconstructed, this does not lead to large strain accumulation. The epitaxial relationship between the KBr and NTCDA lattices (a_{KBr} = $\mathbf{M}\cdot b_{NTCDA}$) is measured to be $\mathbf{M} = \begin{pmatrix} 1.99\pm0.01 & 0\pm0.009 \\ 0\pm0.01 & 0.753\pm0.008 \end{pmatrix}$. Hence, an approximately coincident (all approximately rational values of $\mathbf{M}_{ij}$), or quasi-epitaxial structure, is observed within the error of the measured surface mesh. The film unit mesh orientation on KBr is shown schematically in Fig. 4. Note that for any given matrix alignment with a finite uncertainty, it is almost always possible to find a rational number that lies within this uncertainty. That is, over a large enough "supercell"[16], any lattice will appear to be coincident. For this reason, we maintain the use of the term 'quasi-epitaxy', rather than 'coincident-epitaxy.'

For DB-TCNQ, the (001) orientation on KBr has the DB and TCNQ molecules lying lengthwise on the substrate in alternating parallel rows. Most remarkable is the

fact that these data strongly suggest that the two component growth of DB and TCNQ is almost perfectly congruent[24] similar to what is observed in group III-V and II-VI binary semiconductor alloys. The resulting DB-TCNQ structure is also shown in Fig. 4. The bulk lattice surface mesh of DB-TCNQ (001) is $b_1 = 0.922$nm, $b_2 = 1.064$nm, $\beta = 67.66^{\circ}$. From the RHEED data, we measure $b_1 = 0.91(\pm 0.01)$nm, $b_2 = 1.056(\pm 0.01)$nm, and $\beta = 67(\pm 1.5)^{\circ}$ (note that $\beta = 66.5(\pm 0.5)^{\circ}$ was confirmed from the TEM data) for a layer grown on KBr, which is within error of the bulk phase dimensions. From XRD, we measure an out-of-plane spacing of $d_{(001)} = 0.631(\pm 0.002)$nm, which is also within error of the bulk value of $d_{(001)} = 0.633(\pm 0.001)$nm. That is, while the NTCDA lattice is reconstructed, the DB-TCNQ lattice is not. The measured lattice meshes were identical (within error) to those measured for the first layer of DB-TCNQ grown on NTCDA. The relationship between the KBr and DB-TCNQ lattices can be described by the transformation matrix

$$\mathbf{M} = \begin{pmatrix} 1.38\pm0.02 & 0\pm0.02 \\ 0.63\pm0.03 & 1.47\pm0.02 \end{pmatrix}.$$

The lattice alignment determined from the RHEED data is confirmed by TEM diffraction on a bilayer structure shown in Fig. 5. Although only one orientation was observed for NTCDA in RHEED, two orientations are found to be rotated by 90º in these patterns, although one of the rotations exhibits a very low intensity. These orientations of the NTCDA layer around the KBr lattice are energetically equivalent, and one might expect to see equal distributions along both. However, the diffusive growth conditions in OVPD, along with step edge nucleation may explain the presence of a single preferred alignment. Nonetheless, the exact alignments of DB-TCNQ with respect to the NTCDA

lattice can be deduced from these data which confirmed the values of **M** = $\begin{pmatrix} 0.70 \pm 0.01 & 0 \pm 0.02 \\ 0.32 \pm 0.02 & 1.96 \pm 0.04 \end{pmatrix}$ from RHEED data.

V. DISCUSSION

To further understand the orientation relationships of adlayer to substrate, we calculated both the geometric lattice potential (see Experimental section for description), (V/V_0), and the full atomistic van der Waals potential energy (PE, Θ) between the substrate and the adlayer[14] as a function of substrate-adlayer azimuthal rotation angle (θ). In Fig. 6, the geometric potential tends toward coincidence ($V/V_0 \sim 0.6$) for small NTCDA lattice sizes on KBr at 0º, 90º, and 180º (all symmetrically equivalent). For larger cell sizes the coincidence becomes less substantial ($V/V_0 \sim 0.95$) at 0º. In contrast, the surface potential calculations indicate an energy well (baseline minus bottom of well) of approximately 0.3kcal/mol-nm^2 (this surface energy can be converted to energy/area via Avagadro's number) at 0º that grows deeper and more narrow with a larger number of molecules. The depth of the energy well for a 3*x*3 surface mesh is ~75meV or within 3*kT,* which further indicates a clear route to ordered growth: as the NTCDA nucleates, it can readily sample the energy landscape to find the preferred geometric alignment. As the grain grows, the alignment becomes fixed since the energy cost for rotation increases. In either case, the preferred alignment of both models is consistent with RHEED observations.

For DB-TCNQ grown on KBr (see Fig. 6b), the geometric model fails to predict a preferred angle (i.e. the model predicts incommensurate lattices at every rotation, $V/V_0 \sim 1$), while the surface potential calculations exhibit minima at 0º and 90º consistent with

the RHEED and TEM data. In this case, as the unit cell size increases the potential well depth (baseline minus bottom of well) decreases while the minima remain at the same angles, indicating that grain re-alignment may be active up to larger grain sizes. The depth of the well is significantly smaller, ~0.1kcal/mol-nm^2, than for NTCDA on KBr, indicating a weaker driving force for quasiepitaxial alignment. Regardless, this driving force is sufficient to promote a preferred alignment, as experimentally observed.

For DB-TCNQ deposited on NTCDA, the geometric model indicates one semi-coincident ($V/V_0 \sim 0.6$) alignment at 90.5º (b_1 (DB-TCNQ) || b_2 (NTCDA)) for small cells that disappears for larger surface meshes. In contrast, the surface potential calculations indicate several energy minima for small cell sizes, with the deepest well at 180º. For larger unit cells the number of energy wells reduces to two preferred alignments at 0º and 180º (b_1 (DB-TCNQ) || b_1 (NTCDA)) with a well depth similar to NTCDA of ~0.2kcal/mol-nm^2. Another, shallower well, is observed at 16º (b_2 (DB-TCNQ) || b_2 (NTCDA)). Note that without consideration of the molecular structure (i.e. lattice geometry only) 0º and 180º are symmetric; however, with the full molecular structure these angles are not symmetric due to the subtle molecular tilts in both adlayer and substrate. This results in slightly differing energies between the two orientations, even though the energy barrier between the two is likely to be small, as no azimuthal rotation is required for equivalence. Experimentally, the 0º, 180º orientation is observed, and agrees with the potential energy calculations, while the geometric model failure to predict this alignment is striking.

Potential energy calculations indicate that preferred alignments can be observed for entirely incommensurate organic lattices (e.g. DB-TCNQ on KBr is incommensurate

and DB-TCNQ on NTCDA shows an incommensurate preferred alignment, both with PE calculations and experimentally, even though a semi-coincident orientation theoretically exists). While geometric lattice calculations are sensitive to the precise value of the lattice constants (< ±0.01nm), potential energy calculations showed similar energetic minima for a relatively large range of lattice constants (> ±0.04nm). This, in addition to better experimental azimuthal agreement, highlights the importance of molecular structure over pure lattice geometry in determining the observed quasiepitaxial alignments.

Returning to Fig. 1, we observe that in growing additional alternating-layers the orientation and order are maintained throughout the stack. The azimuthal dependence shown in Fig. 2 is observed for at least 5 pairs of (5nm) NTCDA and (5nm) TCNQ[25]. We find that the choice of the first layer (NTCDA or DB-TCNQ) does not impact the ability to continue with ordered growth. However, starting with NTCDA, the layer roughness was minimized (as observed by the RHEED streak continuity), leading to ordering for a larger number of pairs. While > 5 ordered periods can be grown, the reduction in the streak length into spot-like features (e.g. Fig. 1e, 1g) indicates the evolution of at least some surface roughening. This may be due, in part, to step-edge formation of partially completed MLs leading to an increase in dislocation density with the number of layers. From the RHEED data, we find that the NTCDA b_1 lattice parameter decreases monotonically from 0.497(±0.005)nm in the first layer, to 0.482(±0.005)nm in the second layer, and 0.473(±0.005)nm in the third layer. By comparison, the DB-TCNQ lattice remains unchanged with b_1 = 0.910(±0.010)nm in the first layer, 0.908(±0.01)nm in the second layer, and 0.905(±0.01)nm in the third layer.

Interestingly, the NTCDA lattice becomes more distorted from the bulk phase with each subsequent layer. This behavior is distinct from the neat layer growth of NTCDA on KBr where the lattice constant remained constant. Therefore, the epitaxial structures are related to the energy landscape evolution, which may be different in the presence of the DB-TCNQ as compared to KBr.

Surface energies (similar to the PE discussed above, but summed over interactions within each layer) are indeed important in wetting phenomena. Table II shows the results of calculations of the van der Waals surface energy[26] for various crystalline orientations and materials. Both NTCDA and DB-TCNQ grown on KBr(001) by OVPD form the lowest energy crystalline surfaces of (100) and (001), respectively. This indicates that there are only weak interactions between each layer and the substrate, and between the two organic layers. Comparing the surface energies of the NTCDA(100) and DB-TCNQ(001), we find close agreement of 12.6kcal/mol-nm^2 and 12.1kcal/mol-nm^2, respectively, where other organic systems exhibit surface energies ranging from 9.0kcal/mol-nm^2 to 30.0kcal/mol-nm^2. While it is tempting to point to this surface energy matching as inducing wetting, and hence layer-by-layer growth necessary to obtain smooth and ordered crystals, it may not be the only factor leading to ordered multilayer crystalline growth. Other considerations may include: 1) The crystal orientations have in-plane stacking arrangements that promote crystallization. 2) A clear preferred azimuthal orientation (energetic minimum) exists between the two lattices. 3) The two crystals only weakly interact,[22] resulting in minimal misfit strain at the interface. Nonetheless, our evidence suggests that surface energy plays an important role in

inducing ordered growth across heterointerfaces, in addition to guiding preferred alignments.

VI. CONCLUSIONS

In conclusion, we have demonstrated the quasi-epitaxial growth for NTCDA/DB-TCNQ multilayers on single crystal substrates using organic vapor phase deposition. These two materials are capable of supporting alternating-multilayer single crystalline growth for >5 pairs of NTCDA/DB-TCNQ with a sustained azimuthal crystalline alignment. The organic-organic quasiepitaxial relationship is confirmed by *in-situ* HP-RHEED, *ex-situ* TEM, and potential energy calculations. Additionally, we find a close surface-energy matching between the structures of NTCDA(100) and DB-TCNQ(001), which plays an important role in developing ordered crystalline thin films since it drives layer-by-layer growth that results in flat surfaces required for initiating order in subsequent molecular layers. Factors such as molecularly-flat crystal packing of the lowest energy crystal surface, may also be important.

ACKNOWLEDGEMENT

The authors thank the Department of Energy EERE Program (DE-FG36-08GO18022), Universal Display Corp., and Global Photonic Energy Corp. for their support of this work. M.K. acknowledges the German Academic Exchange Service (DAAD) for generous support within the postdoctoral fellowship program and thanks A Kahn for stimulating discussions on this work.

References

[1] M. Campione, M. Moret, L. Raimondo, et al., J. Phys. Chem. C **113**, 20927 (2009).

[2] H. Akimichi, T. Inoshita, S. Hotta, et al., Appl. Phys. Lett. **63**, 3158 (1993).

[3] G. Koller, S. Berkebile, J. R. Krenn, et al., Nano Lett. **6**, 1207 (2006).

[4] D. Kasemann, C. Wagner, R. Forker, et al., Langmuir **25**, 12569 (2009).

[5] T. Schmitz-Hubsch, F. Sellam, R. Staub, et al., Surf. Sci. **445**, 358 (2000).

[6] L. Z. Huang, F. Zhu, C. F. Liu, et al., Org. Elect. **11**, 195 (2010).

[7] R. R. Lunt, J. B. Benziger, and S. R. Forrest, Adv. Mater. **19**, 4229 (2007).

[8] Here we utilize the term quasi-epitaxy to highlight the nature that organic-inorganic lattices are typically incommensurate and yet show a preferential orientation of the lattice alignments.

[9] S. R. Forrest, P. E. Burrows, E. I. Haskal, et al., Phys. Rev. B **49**, 11309 (1994).

[10] F. F. So and S. R. Forrest, Phys. Rev. Lett. **66**, 2649 (1991).

[11] E. I. Haskal, Z. Shen, P. E. Burrows, et al., Phys. Rev. B **51**, 4449 (1995).

[12] M. T. Jones, R. Kellerman, A. Troup, et al., Chemica Scripta **17**, 43 (1981).

[13] M. Baldo, M. Deutsch, P. Burrows, et al., Adv. Mater. **10**, 1505 (1998).

[14] S. R. Forrest and Y. Zhang, Phys. Rev. B **49**, 11297 (1994).

[15] Calculated using Material Studio *v*4.1.

[16] A. C. Hillier and M. D. Ward, Phys. Rev. B **54**, 14037 (1996).

[17] K. Sakai and M. Hiramoto, Molecular Crystals and Liquid Crystals **491**, 284 (2008).

[18] T. Hasegawa and J. Takeya, Science and Technology of Advanced Materials **10**, 024314 (2009).

[19] Y. Takahashi, T. Hasegawa, Y. Abe, et al., Appl. Phys. Lett. **86**, 063504 (2005).

[20] K. Shibata, K. Ishikawa, H. Takezoe, et al., Appl. Phys. Lett. **92**, 023305 (2008).

[21] Purchased from Sigma Aldrich.

[22] S. R. Forrest, Chem. Rev. **97**, 1793 (1997).

[23] R. R. Lunt, J. B. Benziger, and S. R. Forrest, Appl. Phys. Lett. **90**, 181932 (2007).

[24] C. G. Dekruif and H. A. J. Govers, J. Chem. Phys. **73**, 553 (1980).

[25] As the thickness was reduced to < 2nm for each layer, the RHEED patterns vanished after only several layers, likely due to compositional "intermixing" of the layers similarly seen the pentacene-tetracene system (see Ref. [2]). The "intermixing" in this case has to do with incomplete layer-by-layer growth, where an accumulation of step-edges of unequal height from each material leads to frustration of the crystal arrangement.

[26] D. Winn and M. F. Doherty, AIChE **46**, 1348 (2000).

[27] Crystal structures obtained from the Cambridge Structural Database.

[28] L. F. Drummy, P. K. Miska, D. Alberts, et al., J. Phys. Chem. B **110**, 6066 (2006).

[29] C. Ambrosch-Draxl, D. Nabok, P. Puschnig, et al., New Journal of Physics **11** (2009).

Figure Captions

Figure 1 – High pressure reflection high energy electron diffraction (HP-RHEED) patterns of NTCDA/DB-TCNQ growth on single-crystal KBr by organic vapor phase deposition. (a) HP-RHEED pattern for the KBr substrate scaled by a factor of 0.75*x*. HP-RHEED patterns of the first (b-c), second (d-e), and third (f-e) pair growth of NTCDA(5nm)/DB-TCNQ(5nm). Congruent growth of DB-TCNQ layers (c, e, g) are grown at T_{sub} = 0ºC and r_{dep} = 0.4nm/s on proceeding layers of NTCDA (b, d, f) grown at T_{sub} = 25ºC and r_{dep} = 0.15nm/s. Positions of the diffraction streaks are highlighted by dashed lines. Note that the central streak (c,e,g) separates into multiple streaks indicating surface roughening with increasing number of layers. The electron beam energy and current were 20.0keV and < 0.1μA respectively. (right) Schematic structural model of the multilayer NTCDA (red)/DB-TCNQ (blue,yellow) crystal structure with the individual molecular structures shown in (h); K - maroon, Br – purple, C – grey, O – red, N – blue, S – yellow, and H – white (color online).

Figure 2 - Rotation dependence of RHEED patterns for the first layer of NTCDA(a-c), and the second layer (i.e. 2nd pair) of DB-TCNQ(d-f) for the growth in Fig. 1. The measured *d*-spacings for NTCDA are (a) (10),(20),(30) = 0.491nm, 0.332nm, 0.250nm, respectively, (b) (02), (04) = 0.652nm, 0.331nm, respectively, and (c) (12), (13), (22), (24) = 0.492nm, 0.393nm, 0.240nm, 0.203nm, respectively. The measured *d*-spacings for DB-TCNQ are (d) (10), (30) = 0.849nm, 0.272nm, respectively, (e) (01), (03) = 0.984nm, 0.323nm, respectively, and (f) (11) =

0.805nm. Note that diffraction stemming from the first-order Laue zone in (a) can be observed for NTCDA. The NTCDA alignments are $[10]_N//[100]_{KBr}$, $[01]_N//[010]_{KBr}$, and $[12]_N\sim//[110]_{KBr}$ and the DB-TCNQ alignments are $[10]_D\sim//[130]_{KBr}$, $[01]_D//[010]_{KBr}$, $[11]_D\sim//[320]_{KBr}$.

Figure 3 - X-ray diffraction patterns for single and multilayers of NTCDA and DB-TCNQ. The diffraction peaks in the multilayer structure are a simple convolution of the (100) and (001) peaks seen in the single-layer diffraction for NTCDA and DB-TCNQ. The normal direction alignments of these two lattices are therefore $(100)_N//(001)_D$. Note that multiple diffraction orders (n00) and (00n) are observed for NTCDA and DB-TCNQ, respectively, and the KBr (002) peak is seen at 2θ = 27.80º. (color online)

Figure 4 - Model of the real-space overlayer alignment (a-b) for DB-TCNQ (b, left) and NTCDA (b, right) on KBr diagrammed with (b) and without (a) the molecules in the unit cell; drawings are to scale. In (b), the molecular alignment within the unit cell is assumed from the bulk phase crystal structure. The potassium ions are slightly smaller than the bromine ions, and the KBr unit cell is indicated. The reciprocal lattice vectors (b*) are also highlighted for NTCDA and DB-TCNQ. (color online)

Figure 5 - Transmission electron microscope (TEM) diffraction pattern (a) from an NTCA/DB-TCNQ bilayer transferred from the KBr substrate via aqueous solution

etching. The electron beam is oriented normal the bilayer surface and $(001)_{KBr}$ $//(100)_N//(001)_D$. (b) TEM pattern from (a) overlaid with the measured reciprocal lattice map. Note that slight smearing of the diffraction spots likely stems from a combination of growth-related and wet-transfer induced dislocations. This map is consistent with the picture obtained from HP-RHEED, except that two rotations of NTCDA are observed: one of much lower diffraction intensity and rotated by 90º than the other (this rotation is not observed in HP-RHEED). The alignment of the $[01]_D/[01]_N$ (i.e. b_1(D)// b_1(N))and $(001)_D//(100)_N$ are also consistent with Fig. 3. Note that the diffraction spots yield the *d*-spacing of the surface mesh since the monoclinic/triclinic (*hkl*) reciprocal lattice points lie slightly out-of plane (also leading to a relatively low diffraction intensity). Diffraction data were obtained at a beam energy of 300keV. (color online)

Figure 6 - Van der Waals potential energy (left axis) and geometric lattice potential (V/V_0) (right axis) as a function of adlayer-substrate azimuthal angle (θ) for (a) NTCDA on KBr, (b) DB-TCNQ on KBr, and (c) DB-TCNQ on NTCDA for adlayer surface mesh sizes comprised of 3*x*3 unit cells (orange line) and 15*x*15 unit cells (black line). (b) (Inset) The rotation angle (θ) was defined as the angle between b_1 of the adlayer (b_1^A) and substrate (b_1^S) defined in Fig. 4. Surface lattice parameters for NTCDA and DB-TCNQ were those measured from RHEED data and $a_1 = a_2 = 0.66$nm for KBr. A 6-12 Lennard-Jones potential was used to calculate the PE and only interactions between the substrate and adlayer were included in the summation (surface energies incorporating the summation of intralayer potentials are provided in Table II). Note that 0º and 90º are

symmetrically equivalent for NTCDA and DB-TCNQ on KBr, but not for DB-TCNQ on NTCDA. Measured rotation angles are highlighted with blue arrows. For the dimensionless geometric potential, a value of V/V_0 = 1.0, 0.5, and 0.0 indicates an incommensurate, coincident, and commensurate layer, respectively. Note that simple geometrical lattice considerations do not always elucidate energetic minima necessary to describe quasiepitaxy. (color online)

Table I: 6-12 Lennard Jones constants used in the van der Waals potential energy (PE) calculations; *A* is the atom-atom potential well depth and *B* is interaction distances. Unlike interactions were calculated as $A_{ij} = \sqrt{A_i A_j}$ and $B_{ij} = 1/2\left(B_i + B_j\right)$.

Element	*A* (kcal/mol)	*B* (nm)
C	0.095	0.39
N	0.074	0.37
O	0.096	0.34
S	0.344	0.40
Br	0.370	0.40
K	0.100	0.32

Table II: Calculated surface energies[26] for a range of organic crystals including DB-TCNQ and NTCDA[27]. Values reported for the acenes are similar to those reported elsewhere.[28, 29]

Material	Crystal Plane	Surface Energy (kcal/mol-nm^2)
NTCDA	(001)	21.1
NTCDA	(202)	16.0
NTCDA	(100)[a)]	12.1
DB-TCNQ	$(2\bar{1}0)$	21.2
DB-TCNQ	(010)	13.6
DB-TCNQ	(001) [a)]	12.5
Tetracene	(001) [a)]	14.6
Pentacene	(001) [a)]	14.9
Rubrene	(200) [a)]	12.9
Coronene	$(10\bar{1})$ [a)]	9.2
NPD	(101) [a)]	17.8
C_{60}	(111) [a)]	14.6

a) Lowest energy surfaces.

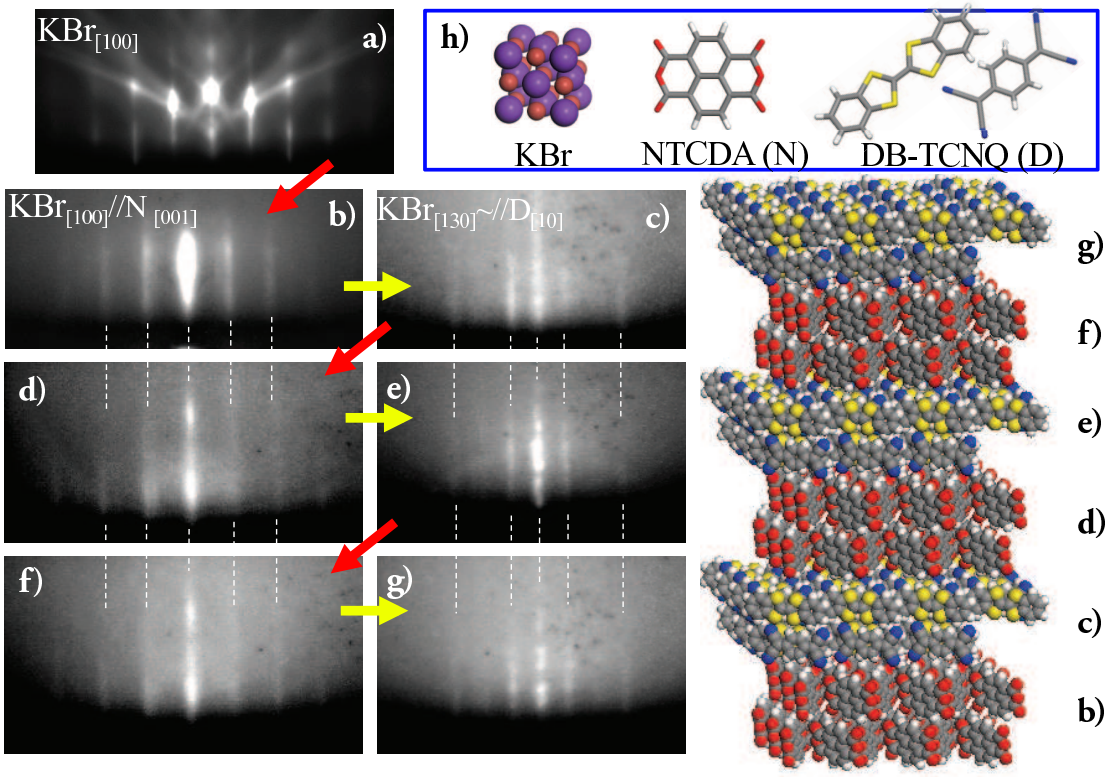

Fig. 1

Figure 1 BU11425 11JAN2011

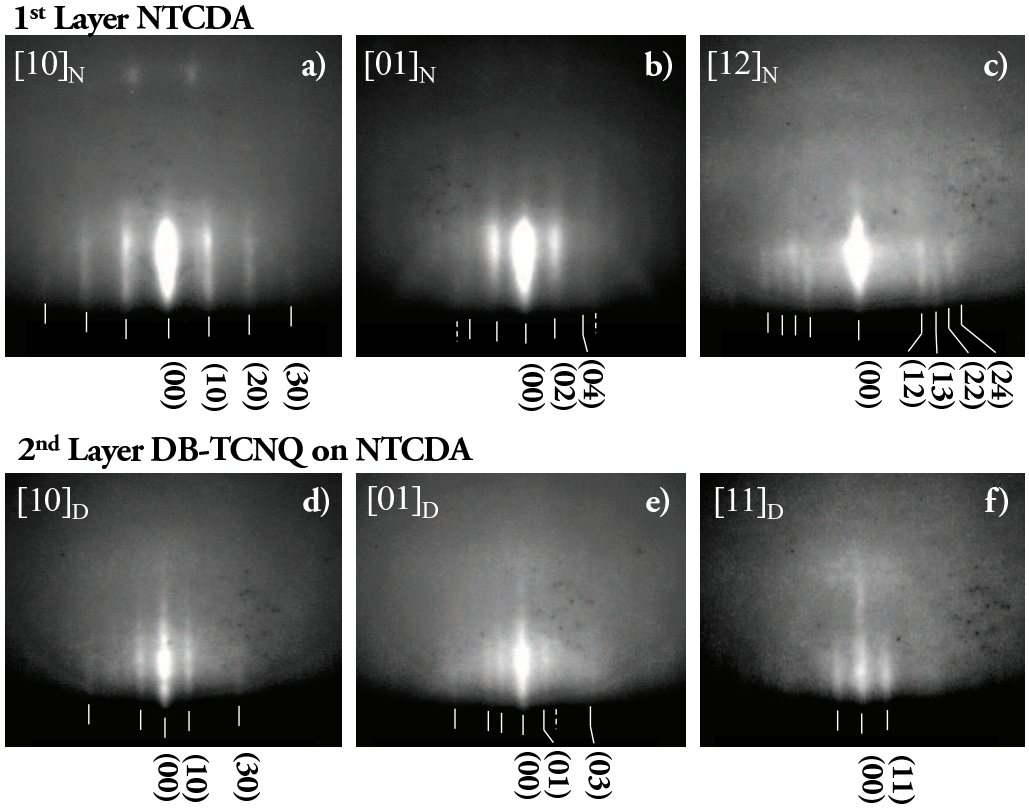

Fig. 2

Figure 2 BU11425 11JAN2011

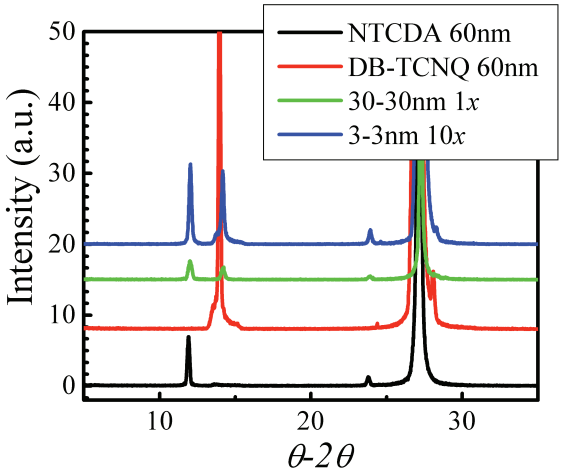

Fig. 3

Figure 3 BU11425 11JAN2011

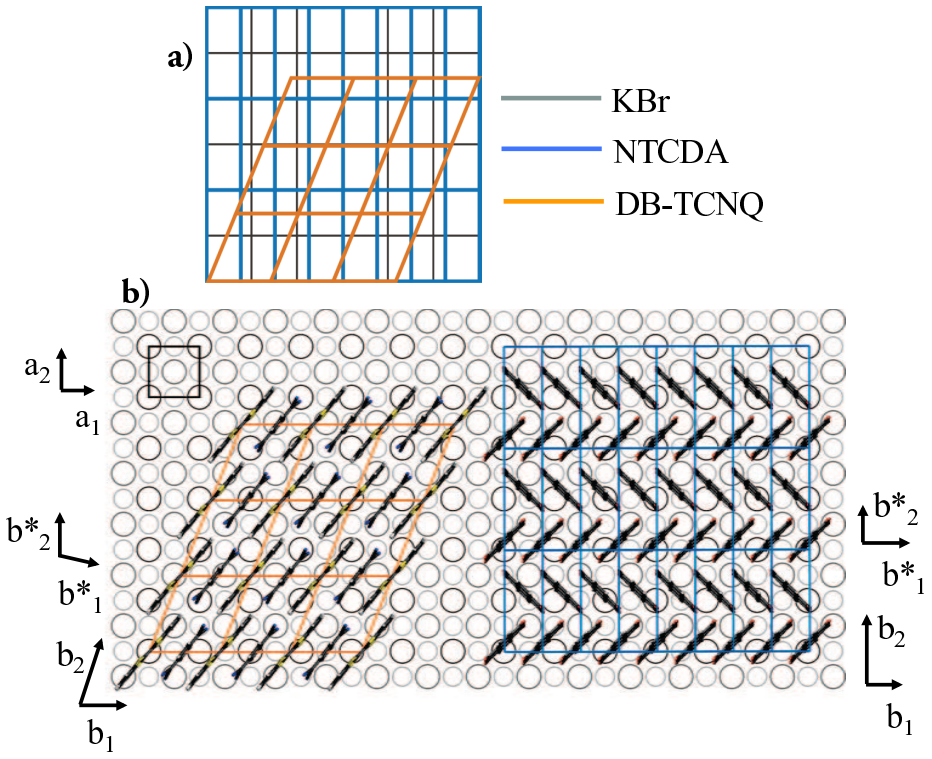

Fig. 4

Figure 4 BU11425 11JAN2011

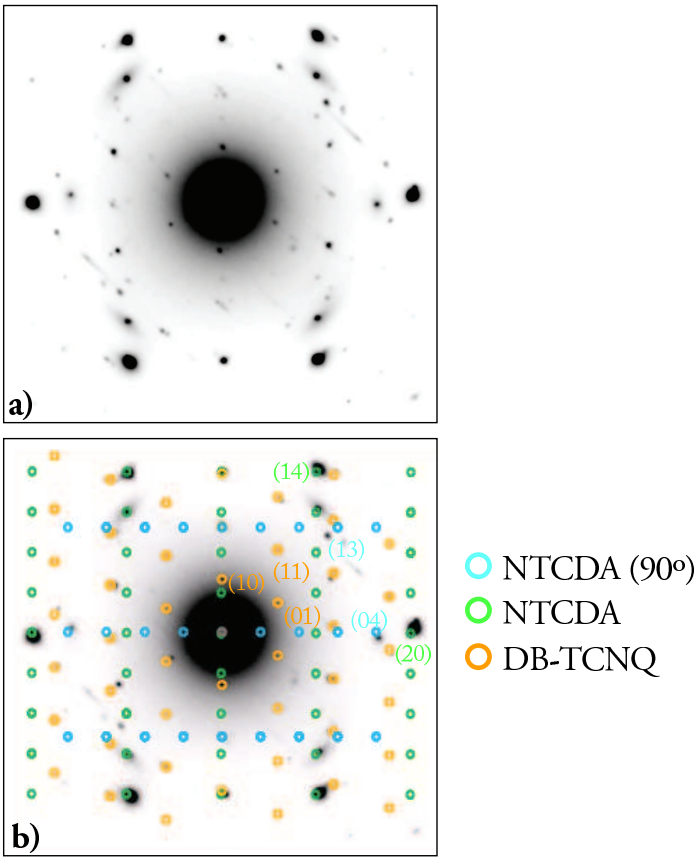

Fig. 5

Figure 5 BU11425 11JAN2011

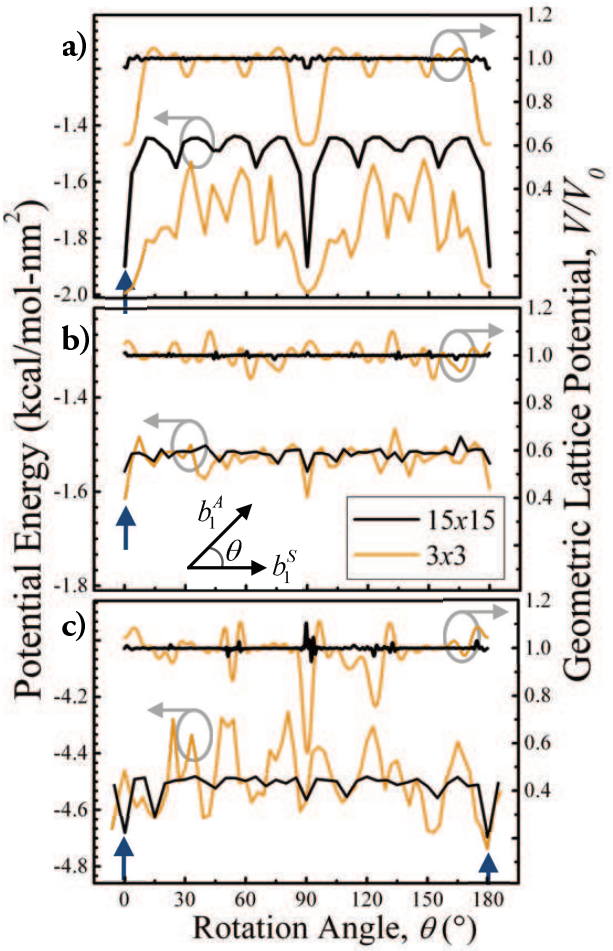

Fig. 6

Figure 6 BU11425 11JAN2011